Article

Cell Reports

PARTICLE, a Triplex-Forming Long ncRNA, Regulates Locus-Specific Methylation in Response to Low-Dose Irradiation

Graphical Abstract

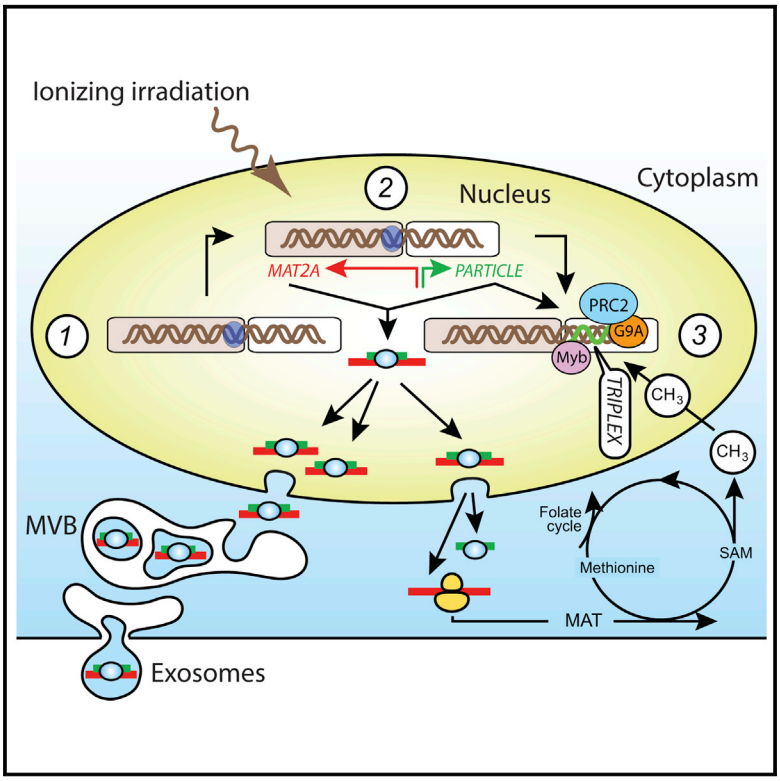

Authors

Valerie Bríd O'Leary, Saak Victor Ovsepian, ..., Michael John Atkinson, Nataša Anastasov

Correspondence

valerie.oleary@helmholtz-muenchen.de

In Brief

O'Leary et al. find a long non-coding RNA called *PARTICLE* that is overexpressed following irradiation. *PARTICLE* represses a tumor suppressor *MAT2A* via triplex formation and interaction with the polycomb repressor complex. *PARTICLE* also acts as a cytosolic scaffold for *MAT2A* in preparation for exosomal transport from the cell.

Highlights

- Expression of tumor suppressor *MAT2A* is regulated by *PARTICLE* via triplex formation
- *PARTICLE* interacts with silencing complexes G9a and PRC2
- *PARTICLE* and *MAT2A* are candidate biomarkers in patient plasma post-radiotherapy
- Inverse dose response of *PARTICLE* challenges the radiation linear non-threshold rule

Accession Numbers

GSE67008

O'Leary et al., 2015, Cell Reports *11*, 474–485
April 21, 2015
http://dx.doi.org/10.1016/j.celrep.2015.03.043

OPEN ACCESS
CellPress

Cell Reports
Article

PARTICLE, a Triplex-Forming Long ncRNA, Regulates Locus-Specific Methylation in Response to Low-Dose Irradiation

Valerie Bríd O'Leary,[1,*] Saak Victor Ovsepian,[2] Laura Garcia Carrascosa,[3] Fabian Andreas Buske,[4,5] Vanja Radulovic,[1] Maximilian Niyazi,[6] Simone Moertl,[1] Matt Trau,[3,7] Michael John Atkinson,[1,8,9] and Nataša Anastasov[1,9]

[1]Institute of Radiation Biology, Helmholtz Zentrum Munich, German Research Center for Environmental Health, Ingolstaedter Landstrasse 1, 85764 Neuherberg, Germany
[2]Deutsches Zentrum für Neurodegenerative Erkrankungen (DZNE), Ludwig-Maximilian-Universität Munich, Zentrum für Neuropathologie, 81377 Munich, Germany
[3]Centre for Personalized Nanomedicine, Australian Institute for Bio-engineering and Nanotechnology, The University of Queensland, Corner College and Cooper Roads, Brisbane, QLD 4072, Australia
[4]Kinghorn Cancer Centre, Garvan Institute of Medical Research, 384 Victoria Street, Darlinghurst, Syndey, NSW 2010, Australia
[5]St. Vincent's Clinical School, University of New South Wales Australia, 390 Victoria Street, Darlinghurst, Sydney, NSW 2010, Australia
[6]Department of Radiation Oncology, Ludwig-Maximilian-Universität Munich, Marchianinistrasse 15, 81377 Munich, Germany
[7]School of Chemistry and Molecular Biosciences, The University of Queensland, Brisbane, QLD 4072, Australia
[8]Chair of Radiation Biology, Technische Universität München, Arcisstrasse 21, 80333 Munich, Germany
[9]Co-senior author
*Correspondence: valerie.oleary@helmholtz-muenchen.de
http://dx.doi.org/10.1016/j.celrep.2015.03.043

SUMMARY

Exposure to low-dose irradiation causes transiently elevated expression of the long ncRNA *PARTICLE* (gene *PARTICLE*, promoter of *MAT2A*-antisense radiation-induced circulating lncRNA). *PARTICLE* affords both a cytosolic scaffold for the tumor suppressor methionine adenosyltransferase (*MAT2A*) and a nuclear genetic platform for transcriptional repression. In situ hybridization discloses that *PARTICLE* and *MAT2A* associate together following irradiation. Bromouridine tracing and presence in exosomes indicate intercellular transport, and this is supported by ex vivo data from radiotherapy-treated patients. Surface plasmon resonance indicates that *PARTICLE* forms a DNA-lncRNA triplex upstream of a *MAT2A* promoter CpG island. We show that *PARTICLE* represses *MAT2A* via methylation and demonstrate that the radiation-induced *PARTICLE* interacts with the transcription-repressive complex proteins G9a and SUZ12 (subunit of PRC2). The interplay of *PARTICLE* with *MAT2A* implicates this lncRNA in intercellular communication and as a recruitment platform for gene-silencing machineries through triplex formation in response to irradiation.

INTRODUCTION

The abundance of long non-coding RNAs (lncRNAs) in the genomes of higher organisms contributed to their initial relegation as irrelevant transcriptional noise emanating from RNA polymerase II infidelity (Struhl, 2007). Defined as RNA transcripts ranging in length from 200 up to ~100,000 bp lacking a significant open reading frame (Bertone et al., 2004), thousands of lncRNAs have been identified by computational transcriptome prediction (Amaral et al., 2011). Recognition of their functional importance arose from the demonstration of their participation in genomic transcriptional control, with influence ranging from a single locus (Wan et al., 2013) to entire chromosomal regions (Chaumeil et al., 2006; Zhang et al., 2007). Regulation may be through association with chromatin complexes in *cis* (Azzalin et al., 2007; Schoeftner and Blasco, 2008) or *trans* (Gupta et al., 2010; Rinn et al., 2007; Tsai et al., 2010). However, for most lncRNAs, their physiological function remains elusive, with some indications of involvement in disease (Huarte and Rinn, 2010) or as responders to genotoxic insults (Özgür et al., 2013).

Ionizing radiation instigates direct macromolecular damage as well as indirect (non-targeted) cellular and tissue stress (Morgan and Sowa, 2015; Pluder et al., 2011). While the DNA damage response is linear with the applied dose, ancillary effects may deviate significantly from linearity (Kadhim et al., 2013). Crucially, these non-targeted reactions to radiation may be more prominent than the direct damage responses at low doses, i.e., milligray range exposure typically encountered in the workplace, during medical imaging, and from natural sources. Thus, low doses may evoke alternative biological responses compared to those emanating from medium- or high-dose exposure (Mullenders et al., 2009; Waldren et al., 2004).

The molecular players known to be involved in the radiation response include lncRNAs and the polycomb repressor complex 2 (PRC2), as mediators coordinating cellular repair (Campbell et al., 2013; Wang et al., 2008). While the mechanistic role of PRC2 itself in DNA damage signaling must be elucidated,

lncRNAs are becoming recognized as important participants in PRC2 recruitment with their tertiary structure key to specific target gene recognition (Margueron and Reinberg, 2011). LncRNAs such as *lincRNA-p21* and *PANDA* are upregulated by DNA damage as direct targets of p53 (Hung et al., 2011). Regulation of Cyclin D1 (*CCND1*) following ionizing radiation has been demonstrated as a target for promoter-derived lncRNAs, e.g., *ncRNA- CCND1s* (Wang et al., 2008). *ANRIL* (antisense non-coding RNA in the INK4 locus) is overexpressed following high-dose irradiation (5 Gy exposure), which may be related to suppression of senescence by p16 (Özgür et al., 2013). However, limited knowledge exists on the mechanistic response of lncRNAs to ionizing radiation and, in particular, the influence of dose and cellular context (Özgür et al., 2013).

Here we introduce the lncRNA *PARTICLE* (HUGO gene nomenclature *PARTICLE*, promoter of *MAT2A*-antisense radiation-induced circulating lncRNA, NCBI reference sequence NR_038942.1), which demonstrates a substantial increase in expression after low-dose radiation. *PARTICLE* is located within the *MAT2A* gene that encodes the catalytic subunit of methionine adenosyltrasferase (MAT), the enzyme responsible for the production of s-adenosylmethionine (SAM), which is the principal methyl donor of the cell (Mato et al., 1997). Co-localization of *PARTICLE* and *MAT2A* cytosolic transcripts potentially destined for export via exosomes in response to irradiation is demonstrated. We provide evidence that nuclear *PARTICLE* is a suppressor of *MAT2A* through triple helix formation and provides a methyltransferase and polycomb repressor complex recruitment platform. Broadly, our work identifies a potential mammalian riboswitch previously discovered in bacteria, and it suggests that lncRNAs subsequently have been exploited for roles in metabolomic regulation.

RESULTS

PARTICLE Expression Is Modulated by Exposure to Low-Dose Irradiation

Microarray analysis provided an initial platform for target discovery. While ~50 radiation-regulated candidates were identified (Table S1), four lncRNAs (*NR_027405*, *BC036914*, *BX647881*, and *PARTICLE* [*NR_038942.1*]) associated with genes (*MTHFD2*, *GNAII*, *TFDP2* and *MAT2A*, respectively) were selected for further verification by Taqman QPCR assays (see Table S2 for primers and probes). Fold differences in the relative expression of these lncRNAs as well as *PANDA* (*NR_109836.1*, serving as a positive indicator of radiation exposure [Hung et al., 2011]) were initially assessed in T47D, a mammary cancer cell line (due to previous inclusion of this cell line in the high-throughput microarray analysis), at 4 and 24 hr after exposure to 2.5 Gy and in sham-irradiated controls (Figure 1A). No significant changes in expression were found for any of these lncRNAs at 4 hr after 2.5 Gy exposure (Figure 1A; $p > 0.05$). However, at 24 hr, significant increases were noted for the lncRNAs *BX647881* and *PARTICLE*. *BX647881*, associated with *TFDP2*, increased by 3.48 ± 0.11 relative to sham-irradiated controls ($p = 0.001$). There was a more substantial increase of *PARTICLE*, associated with *MAT2A*, at 24 hr after 2.5 Gy irradiation (12.8 ± 2.6-fold compared to controls, $p = 0.02$, as tested in three independent experiments).

These lncRNA expression findings in the relatively radiation-resistant T47D cell line (Anastasov et al., 2012) prompted their further assessment in MDA-MB-361, a radiation-sensitive mammary cancer cell line (Anastasov et al., 2012; Figure 1B). This analysis highlighted different transcriptional responses for these lncRNAs between T47D and MDA-MB-361 and also may reflect alternative RNA steady-state levels. LncRNAs *BC036914*, *PANDA*, *BX647881*, and *PARTICLE* showed significantly enhanced transcription following irradiation (Figure 1B). A robust elevation in *PARTICLE* (27 ± 0.64-fold increase versus control values normalized to unity) was noted, especially 24 hr after 0.25 Gy low-dose irradiation exposure in MDA-MB-361 ($p = 0.00028$; Figure 1B). Increased levels for *PARTICLE* at 4 hr (12 ± 0.1-fold, $p = 0.00056$; Figure 1B) also were noted. While unchanged *PARTICLE* levels were found in sham-irradiated and 2.5 Gy-irradiated samples when analyzed at 4 hr, increased transcription occurred by 24 hr after 2.5 Gy in both T47D and MDA-MB-361 ($p < 0.05$; Figures 1A and 1B). To determine whether the increase in *PARTICLE* transcription due to irradiation was solely restricted to cancer cells, its expression also was assessed in three non-cancerous human cell lines (MCF10A, HUVEC, and HEK293). Enhanced levels of *PARTICLE* following low-dose irradiation were found in all three additional cell lines examined (Figures S1A–S1C), confirming *PARTICLE* to be a ubiquitous tissue responder to low-dose irradiation exposure, irrespective of malignant status or lineage.

A Relationship of *PARTICLE* with the *MAT2A* Gene Is Revealed by the Time Course of the Transcript Expression Pattern following Low-Dose Irradiation

Real-time qPCR analysis of *PARTICLE*, *MAT2A*, and *GGCX* transcription was undertaken at 4, 24, 48, and 72 hr after an acute exposure to 0.25 Gy or 2.5 Gy in MDA-MB-361 cells (Figures 1C–1E). Following 0.25 Gy irradiation, results showed increased *PARTICLE* transcript presence at 4 hr (8.79 ± 0.5-fold increase) in comparison with sham-irradiated experimental controls ($p = 0.004$). *PARTICLE* transcription continued to rise, peaking at 24 hr (20.17 ± 1.6-fold greater than controls, $p = 0.006$; Figure 1C). By 48 hr, *PARTICLE* transcript levels decreased back down toward control cell levels. Of note was the slightly different *PARTICLE* expression profile after the higher (2.5 Gy) dose of radiation. Levels were comparable to controls at 4 hr ($p > 0.05$), with a peak increase of 8.9 ± 1.2-fold at 24 hr ($p = 0.03$) that diminished 5 ± 0.38-fold by 48 hr ($p = 0.018$). The transcriptional decrease continued to 72 hr, reaching non-significance by that time ($p = 0.2$; Figure 1C).

The expression of *MAT2A* transcripts was analyzed due to the genomic co-localization of the *PARTICLE* and *MAT2A* genes. Dramatic elevation of *MAT2A* levels was determined at 4 hr post-irradiation (Figure 1D), while from 24 hr onward to 72 hr *MAT2A* transcripts in 0.25- and 2.5 Gy-irradiated samples showed levels comparable to sham-irradiated controls. There was a significant 6.2 ± 0.9 or 6.9 ± 2.3-fold increase over controls in *MAT2A* transcription following exposure to 0.25 Gy or 2.5 Gy irradiation ($p = 0.001$, $p = 0.03$, respectively) at this time point (Figure 1D). The proximity of *GGCX* to the *PARTICLE*/*MAT2A* locus prompted the assessment of potential variation in *GGCX* transcription during the radiation response.

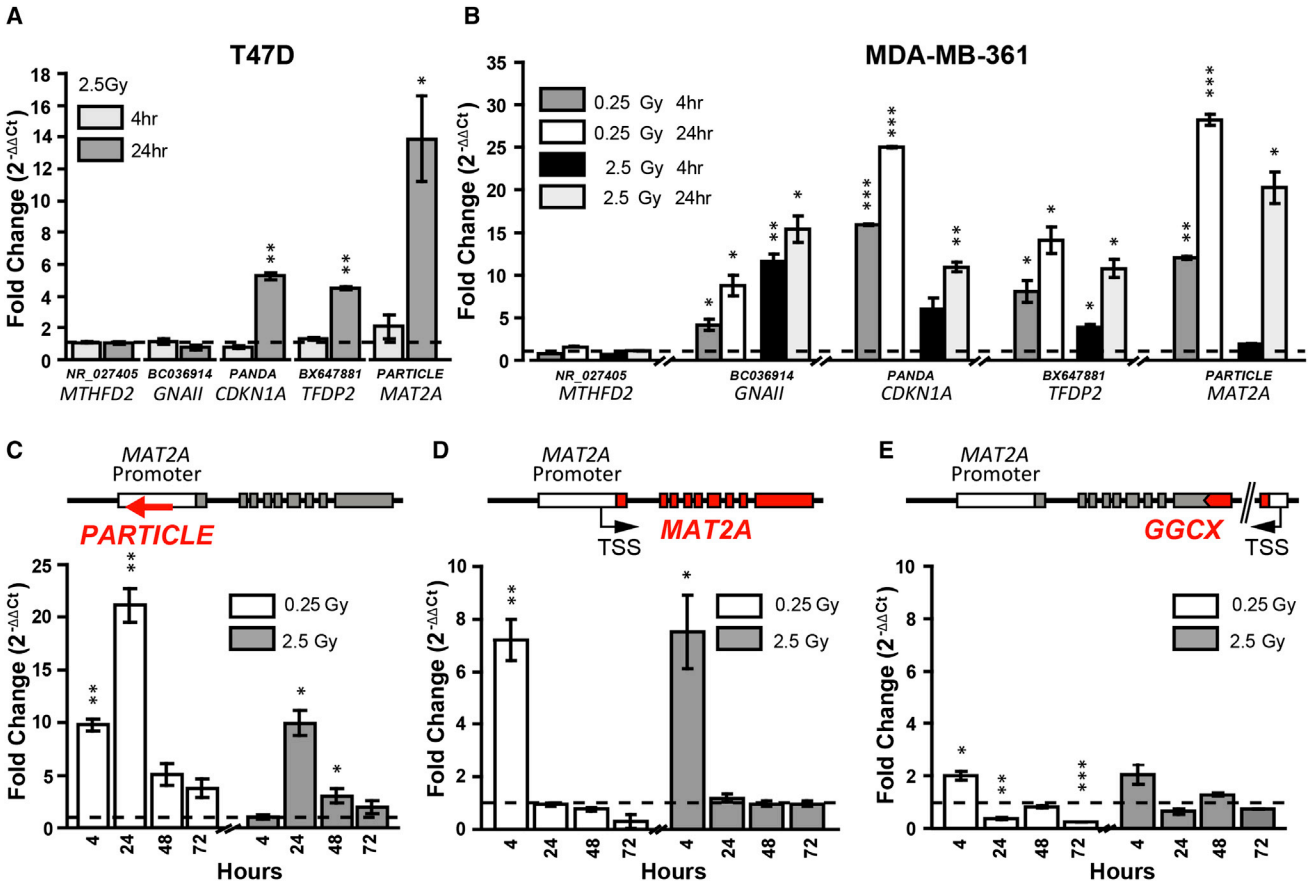

Figure 1. Characterization of lncRNA Transcripts following Low-Dose Irradiation

(A) Histogram shows lncRNAs (*NR_027405*, *BC036914*, *PANDA*, *BX647881*, and *PARTICLE*) expression in T47D, 4 and 24 hr after exposure to 2.5 Gy. Genes associated with each lncRNA are indicated.

(B) Histogram shows lncRNAs (*NR_027405*, *BC036914*, *PANDA*, *BX647881*, and *PARTICLE*) expression plus associated genes (as above) in MDA-MB-361 (radiation-sensitive cell line) 4 and 24 hr after exposure to 0.25 or 2.5 Gy irradiation.

(C–E) Schematic diagram (top) and time course (bottom) of the relative expression of *PARTICLE* (red, C), *MAT2A* (red, D), and *GGCX* (red, E) 4–72 hr following either 0.25 or 2.5 Gy irradiation in MDA-MB-361 with values at 0 Gy taken as a value = 1 (dashed line) for comparative purposes. Data are represented as mean ± SEM with significance represented by asterisks ($p < 0.05$) where appropriate. See also Figure S1 and Tables S1 and S2.

Modest fluctuations in *GGCX* transcription were found after 0.25 Gy exposure (Figure 1E). As there was only a modest relationship with exposure or *PARTICLE*, GGCX was not followed further in this study.

Increased *PARTICLE* Expression in Both the Nucleus and Cytoplasm Is Associated with *MAT2A*

In situ hybridization utilizing fluorescently labeled FAM probes complementary to *PARTICLE* in MDA-MB-361 confirmed that low-dose irradiation induced elevated *PARTICLE* levels (Figures 2A–2C). Substantially increased intensity of *PARTICLE* staining was noted in both the nucleus and cytoplasm 24 hr following 0.25 Gy irradiation (Figures 2A–2C, middle). At the same time point, elevated levels of *PARTICLE* also were noted in these cells after 2.5 Gy exposure compared to controls (Figures 2A–2C, top), although transcripts appeared to be mainly restricted to the cytoplasm with levels not reaching those seen following the lower dose of irradiation. In sham-irradiated cells, *PARTICLE* (green fluorescence) was spatially discreet from *MAT2A* (red fluorescence) transcripts, with both the nucleus and cytoplasm having minimum co-localization (yellow) (Figures 2D–2F). Intriguingly, *PARTICLE* and *MAT2A* transcripts were seen to associate together as early as 4 hr after low-dose irradiation. Regions-of-interest analysis highlighted the increase in the co-localization coefficient in both nuclear and cytoplasmic zones (Figures 2D–2F).

Bromouridine RNA Tracing, Exosomes, and Radiotherapy Patient Plasma Analysis Support the Intercellular Transport of *PARTICLE* following Irradiation

Following transwell relocation, extraction, and north-western detection, RNA labeled with 5-bromouridine (BruU) was noted in recipient MDA-MB-361 exposed for 4 or 24 hr to BruU-labeled irradiated (0.25 Gy) donor cells (Figures 3A and 3B). An increase in the size range of Bru-labeled RNA with time was noted.

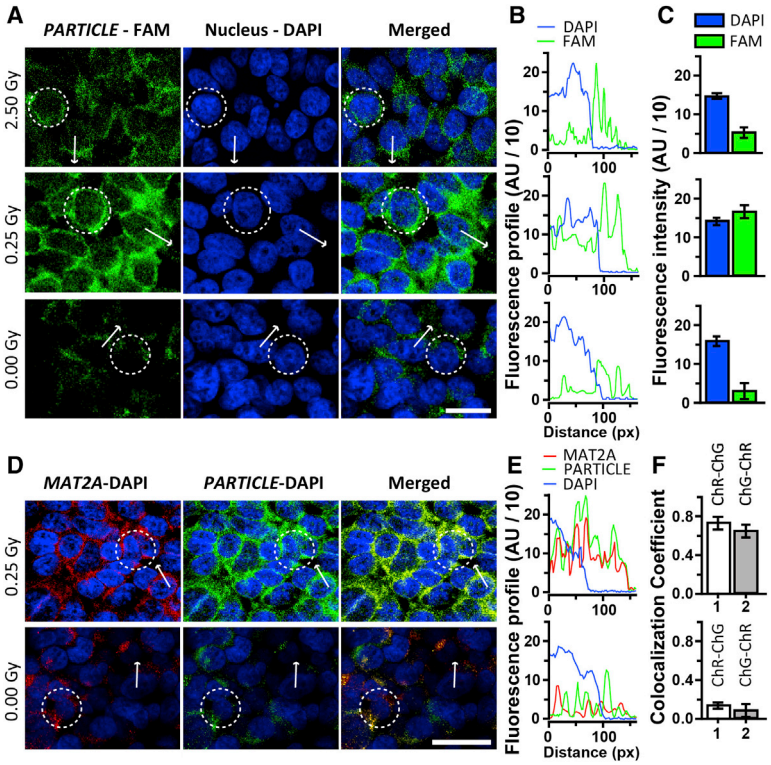

Figure 2. Increased Expression of *PARTICLE* and Co-localization with *MAT2A* following 0.25 Gy Irradiation

(A) Representative confocal microscopic images of MDA-MB-361 24 hr after 2.5 Gy (left, upper), 0.25 Gy (left, middle), or sham irradiation (left, lower) labeled with RNA in situ hybridization probes specific for *PARTICLE* (fluorophore FAM, green, left). Nuclei are stained with DAPI (blue, center). Merged images are shown for *PARTICLE* (green, FAM) and nuclei (blue, DAPI) (right). Representative arrows indicate the position of the transept selected for cross-sectional analysis. Mean fluorescence intensity analysis was determined from regions of interest (ROIs) indicated by circular dashed lines. Scale bar, 20 μm.

(B) Plots of arbitrary units (AUs) of fluorescence profiles of DNA (DAPI, blue line) and *PARTICLE* (FAM, green line) after 2.5 Gy (top), 0.25 Gy (middle), or sham irradiation (bottom). Note, the intracellular localization of *PARTICLE* within the nucleus and cytoplasm as well as it's increased expression following 0.25 Gy compared to 2.5 Gy exposure or sham irradiation.

(C) Summary plots illustrate average fluorescence intensities pooled from the selected ROIs from the various experimental groups.

(D) Representative confocal images of *MAT2A* (red, left) and *PARTICLE* (green, middle) transcripts detected with specific RNA in situ hybridization probes labeled with Quasar570 or FAM, respectively, in MDA-MB-361, 4 hr after 0.25 Gy irradiation (top) or sham irradiation (bottom). Cells were counterstained with DAPI (blue). Merged images of *MAT2A* and *PARTICLE* show co-localization (yellow, right). Scale bar, 50 μm.

(E) Plots of AUs of fluorescence profile of DAPI (blue line), FAM (green line), and Quasar570 (red line) representing nuclei, *PARTICLE*, and *MAT2A*, respectively, 4 hr after 0.25 Gy (top) irradiation or sham irradiation (bottom) are shown.

(F) Summary plots for Quasar570 (ChR, red channel)/FAM (ChG, green channel) and ChG/ChR co-localization in ROI (circular dashed lines in D). Data are represented as mean ± SEM.

PARTICLE was detected by northern blotting of Bru-labeled RNA in recipient cells (Figure 3B).

PARTICLE levels were significantly elevated in exosomes isolated from the media of MDA-MB-361 exposed to 0.25 Gy (1.8 ± 0.05-fold over sham-irradiated controls = 1, p = 0.0008) and to a lesser extent following 2.5 Gy exposure (0.6 ± 0.07-fold versus controls, p = 0.005; Figure 3C). A concomitant enhancement of *MAT2A* transcripts also was noted in extracellular exosomes after the low-dose (0.25 Gy) exposure (1.7 ± 0.2-fold, p = 0.012) with non-significant levels reached after 2.5 Gy irradiation for this gene (0.47 ± 0.28-fold, p = 0.23; Figure 3C). Substantial upregulation of *PARTICLE* expression in T47D following exposure to exosomes isolated from irradiated MDA-MB-361 (24 hr after 0.25 Gy) was noted (35 ± 3.2-fold, p = 0.006; Figure 3D), but was not evident for *MAT2A* (Figure 3E). In vitro exposure of whole blood to 2 Gy with exosomal isolation revealed that, although *PARTICLE* levels varied among individuals, increases ranged from 4.4 ± 0.38- to 22.3 ± 1.8-fold over control levels (p < 0.005; Figure 3F). Likewise, *MAT2A* mRNA also was detected in these exosomes with significantly elevated levels, ranging from 3 ± 0.09- to 4.3 ± 0.6-fold over controls for all exosomal extracts (n = 3; p < 0.05; Figure 3F). Increases in *PARTICLE* also were noted in plasma samples obtained from three of four post-radiation therapy patients (Patients A–C, p < 0.05; Figure 3G). Concomitant increases in *MAT2A* over controls also were revealed (A, 5 ± 0.9-fold, p = 0.014; B, 1.85 ± 0.11-fold, p = 0.002; C, 2.2 ± 0.5-fold, p = 0.01; D, 1.3 ± 0.23-fold, p = 0.01; Figure 3G).

PARTICLE Silencing Enhances *MAT2A* Transcription

Knockdown of *PARTICLE* (Figure S3) caused overexpression of *MAT2A* in sham-irradiated MDA-MB-361 cells (Figure 4A). *PARTICLE* expression was decreased (86.3%, p = 0.002) when MDA-MB-361 were transduced with lentivirus encoding the silencing small hairpin RNA (shRNA)_A compared to empty vector alone (similar to the effects of Cisplatin exposure, Figure S4). At the same time, a reverse trend toward a 2.2-fold elevation was detected in *MAT2A* (p = 0.06). In cells transfected with lentivirus encoding shRNA_B, *PARTICLE* expression was again strongly decreased (94.2%, p = 0.00001) and again coincided with a concomitant 3.3-fold increase in *MAT2A* transcript expression (p = 0.001; Figure 4A).

Expression of *MAT2A* Is Enhanced in *PARTICLE* Knockdown Cells following Low-Dose Radiation Exposure

Knockdown of *PARTICLE* with lentivirus encoding shRNA_B resulted in an overshoot of *MAT2A* expression (7.7-fold increase, p = 0.0038) following low-dose (0.25 Gy) irradiation in MDA-MB-361 cells (Figure 4B). Essentially similar results were seen with

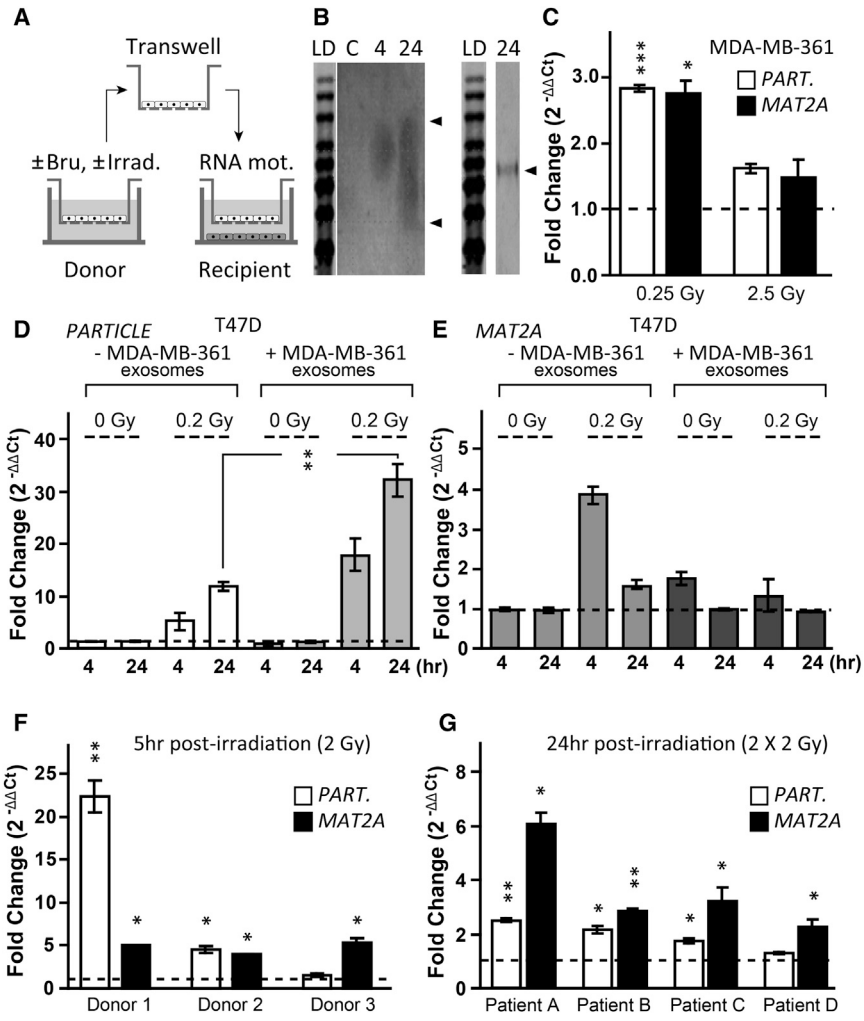

Figure 3. Extracellular Transport of *PARTICLE*

(A) Schematic of experimental overview. After 4 or 24 hr, RNA motility (mot.) was tested in recipient cells.

(B) (Left) North-western blot shows RNA isolated from recipient cells exposed to bromouridine (Bru) RNA labeled and irradiated (4 or 24 hr after 0.25 Gy) donor cells. (Lane 1) RNA size ladder (LD, Ambion); (lane 2) RNA from control (C); (lanes 3 and 4) Bru-labeled RNA isolated from recipient cells (300 and 3,000 bp lower and upper arrowheads). (Right) Northern blot shows *PARTICLE* detected in isolated Bru-labeled RNA in recipient cells exposed to Bru RNA labeled and irradiated (24 hr after 0.25 Gy) donor cells. (Lane 1) RNA ladder (as above); (lane 2) band showing *PARTICLE* (size 1,432 bp, arrowhead).

(C) Plots show fold change in *PARTICLE* and *MAT2A* transcripts in exosomes isolated from tissue culture supernatant 24 hr after 0.25 Gy or 2.5 Gy exposure. Dotted line represents sham-irradiated control values. Note significantly enhanced presence of *PARTICLE* and *MAT2A* after 0.25 Gy (asterisks).

(D and E) Expression of *PARTICLE* (D) and *MAT2A* (E) in T47D following exposure to exosomes isolated from irradiated MDA-MB-361 (24 hr after 0.25 Gy) is shown.

(F) Plots show fold change in *PARTICLE* and *MAT2A* transcripts 5 hr after in vitro irradiation (2 Gy) of blood taken from healthy donors (1–3).

(G) *PARTICLE* and *MAT2A* transcript analysis of plasma taken from head and neck cancer patients (A–D) 24 hr after receiving the second 2 Gy fraction of localized therapeutic irradiation. Dotted line normalized to one represents the control value for each patient before irradiation treatment. Data are represented as mean ± SEM and the asterisks represent significant values ($p < 0.05$). See also Figure S2.

shRNA_A, resulting in *MAT2A* elevation (5-fold, $p = 0.017$; Figure 4B, right). Cells exposed to 2.5 Gy showed similar effects to sham-irradiated cells for *PARTICLE* and *MAT2A* transcription response (Figure 4C). *PARTICLE* expression decreased (62.4%, $p = 0.017$) in MDA-MB-361 cells infected with lentivirus encoding shRNA_A. This again correlated with a 0.5-fold significant increase in *MAT2A* ($p < 0.05$; Figure 4C, right). Slight improvement in *PARTICLE* knockdown was seen (71.6%, $p = 0.0004$) in cells infected with lentivirus encoding shRNA_B, coinciding with a greater, 2.5-fold, significant increase in *MAT2A* ($p = 0.0029$; Figure 4C, right). The increase in *MAT2A* expression was far greater following 0.25 Gy low-dose irradiation compared to 2.5 Gy exposure (5.2-fold higher, $p < 0.005$). These findings highlight the different transcriptional response profiles emanating from exposure to either low or medium irradiation dosage, and they emphasize the homeostatic repressive influence of *PARTICLE* on *MAT2A* expression.

PARTICLE Represses *MAT2A* Promoter Activity

Enhanced *MAT2A* promoter activity was noted in MDA-MB-361 with *PARTICLE* knockdown (Figure 4D, left). While non-transfected (NT) cells showed expectedly negligible luciferase reporter expression, the transcriptional activity was significantly elevated in sham-irradiated cells and following 4 or 24 hr irradiation (0.25 or 2.5 Gy) in the absence of *PARTICLE,* when compared to normal MDA-MB-361 ($p < 0.005$). The highest levels were noted at 24 hr after 0.25 Gy irradiation compared to sham-irradiated *PARTICLE* knockdown cells ($p = 0.0027$). These results again suggest the negative regulation of *MAT2A* promoter activation by *PARTICLE*, coinciding with the time point when *MAT2A* levels decrease (24 hr post-irradiation) and *PARTICLE* levels increase.

Low-Dose Irradiation Promotes the Expression of the Catalytic Subunit of MAT and SAM Production

As previous results revealed elevated *MAT2A* transcription within 4 hr of low-dose irradiation exposure, an investigation was undertaken to determine whether this would have an influence on MAT2A and SAM (Figure 5A). MAT2A in irradiated and sham-irradiated MDA-MB-361 was monitored over time (4–48 hr), revealing an increased concentration of the catalytic subunit of MAT 4 hr post-exposure to 0.25 Gy irradiation

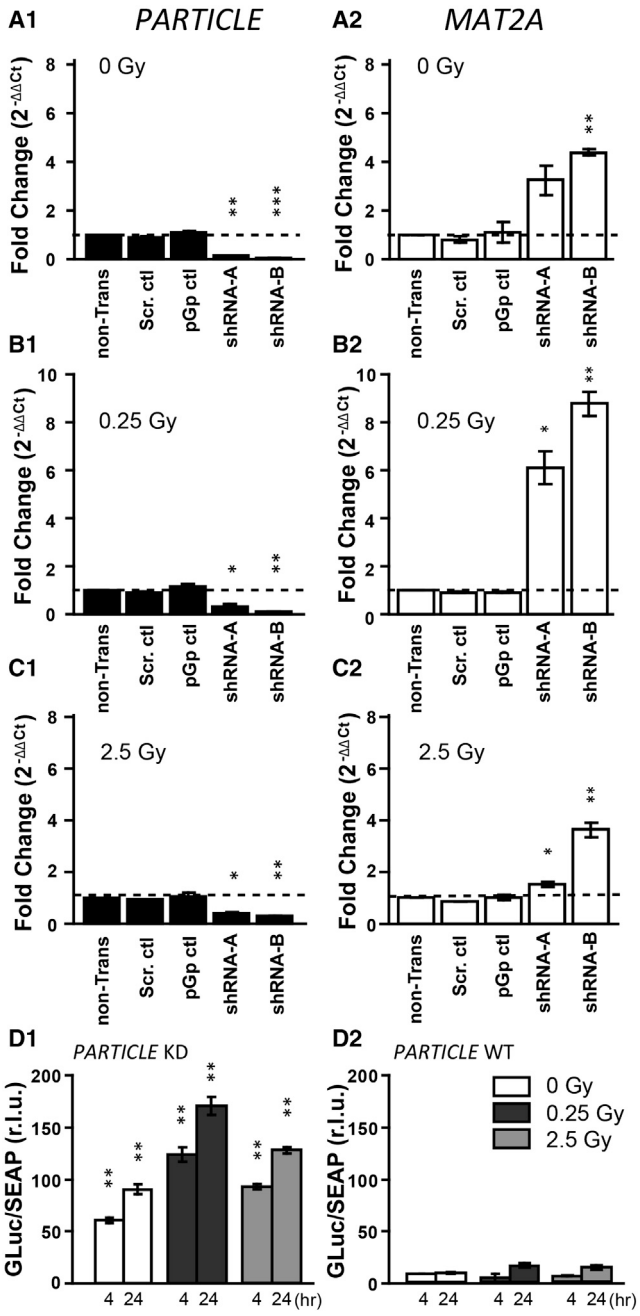

Figure 4. *PARTICLE* Knockdown through Stable Lentiviral Transfection Causes *MAT2A* Overexpression and Promoter Over-activity

(A–C) Plots show fold change in *PARTICLE* (black histograms) and *MAT2A* (white histograms) expression relative to NT (non-Trans.) control levels (dotted line) in MDA-MB-361 that were sham irradiated (A) or exposed to 0.25 Gy (B) or 2.5 Gy (C). *PARTICLE* and *MAT2A* levels in MDA-MB-361 infected with lentivirus expressing non-specific (scrambled) control sequence (slight irradiation effect noted following 2.5 Gy) designed from shRNA_B region (red arrow [Figure S2], Scr. ctl.), pGP vector control (pGP ctl.), shRNA_A (lenti_shRNA_A), or shRNA_B (lenti-shRNA_B) are shown. Data are represented as mean ± SEM with significant levels ($p < 0.05$) indicated where appropriate (asterisks). Note the presence of puromycin in the media did not have an effect on *PARTICLE* or *MAT2A* expression.

($p < 0.05$; Figure 5B). The rapid decrease in MAT2A protein levels by 24 hr post-irradiation exposure ($p < 0.05$; Figure 5B) also reflects the transcriptional expression profile (Figures 1 and 2). Such effects were not evident after exposure to 2.5 Gy, although a trend toward a decrease was apparent at the 24 hr time point, consistent with RNA levels. No alteration in MAT2A was found after 48 hr (Figure 5B), indicative of the transient response of this catalytic subunit specifically to low-dose irradiation exposure.

Intracellular levels of SAM varied from 12 ± 0.15 to 6.5 ± 1.5 nM/10^6 MDA-MB-361 when measured between 4 and 24 hr after sham irradiation (Figure 5C, left). While no effects were noted in MDA-MB-361 up to 48 hr after the 2.5 Gy dose of irradiation, SAM concentrations were twice as high at 4 hr after the low-dose (0.25 Gy) exposure, with levels returning to normal values by 24 hr (Figure 5C).

PARTICLE Knockdown and Irradiation Have an Additive Effect on Intracellular and Extracellular SAM Production

PARTICLE knockdown and concomitant elevation of MAT2A affected intracellular SAM levels in sham-irradiated cells. Significantly elevated SAM levels were noted for both the 4- and 24-hr time points, with concentrations 4- to 5-fold higher than transduced control cells ($p < 0.005$; Figure 5D, left). Following low-dose irradiation, a further substantial increase in intracellular SAM (80 ± 2.76 nM/10^6 cells) was noted in *PARTICLE* knockdown MDA-MB-361 (4-fold SAM increase over NT cells, $p < 0.0005$; Figure 5D, middle). This was only noticeable by 4 hr post-irradiation, particularly following low-dose exposure.

The concentration of extracellular SAM was assessed in the tissue culture medium conditioned by non-transduced or *PARTICLE* knockdown MDA-MB-361 plus or minus irradiation exposure. SAM concentrations in growth medium obtained from sham-irradiated cells varied from 9 ± 0.5 to 7 ± 0.12 nmol/l when collected at 4 to 48 hr after sham irradiation (Figure 5E, left). Significantly increased extracellular SAM levels were identified in the media of MDA-MB-361 exposed 4 hr earlier to low-dose (0.25 Gy) irradiation ($p < 0.05$; Figure 5E, middle). No significant alteration in extracellular SAM levels was found in media taken from cells 4–48 hr previously exposed to 2.5 Gy (Figure 5E, right).

SAM concentrations also were examined in the growth media of MDA-MB-361 in which *PARTICLE* had been depleted by lentiviral shRNA expression (Figure 5F). While no significant difference was found for extracellular SAM levels in sham-irradiated cells (Figure 5F, left), dramatically elevated SAM concentrations (24.7 ± 3 nmol/l) were identified in media from MDA-MB-361 (with *PARTICLE* knockdown) exposed 4 hr earlier to 0.25 Gy. SAM levels subsequently declined to values close to the normal range (6 ± 0.2 nmol/l) by 24 hr, remaining relatively unchanged up to 48 hr post-exposure (5 ± 0.7 nmol/l; Figure 5F, middle). A comparable trend was noted following 2.5 Gy exposure under similar culture conditions. Elevated SAM (13 ± 2.6 nmol/l,

(D) Histogram shows *Gaussia* luciferase (GLuc) secretion normalized to secreted alkaline phosphatase (SEAP) indicative of *MAT2A* promoter activity in MDA-MB-361 (±PARTICLE knockdown [KD]). Tissue culture media were analyzed 4 and 24 hr following 0.25 Gy or 2.5 Gy cellular irradiation or sham irradiation. Data are represented as mean ± SEM. See also Figures S3 and S4.

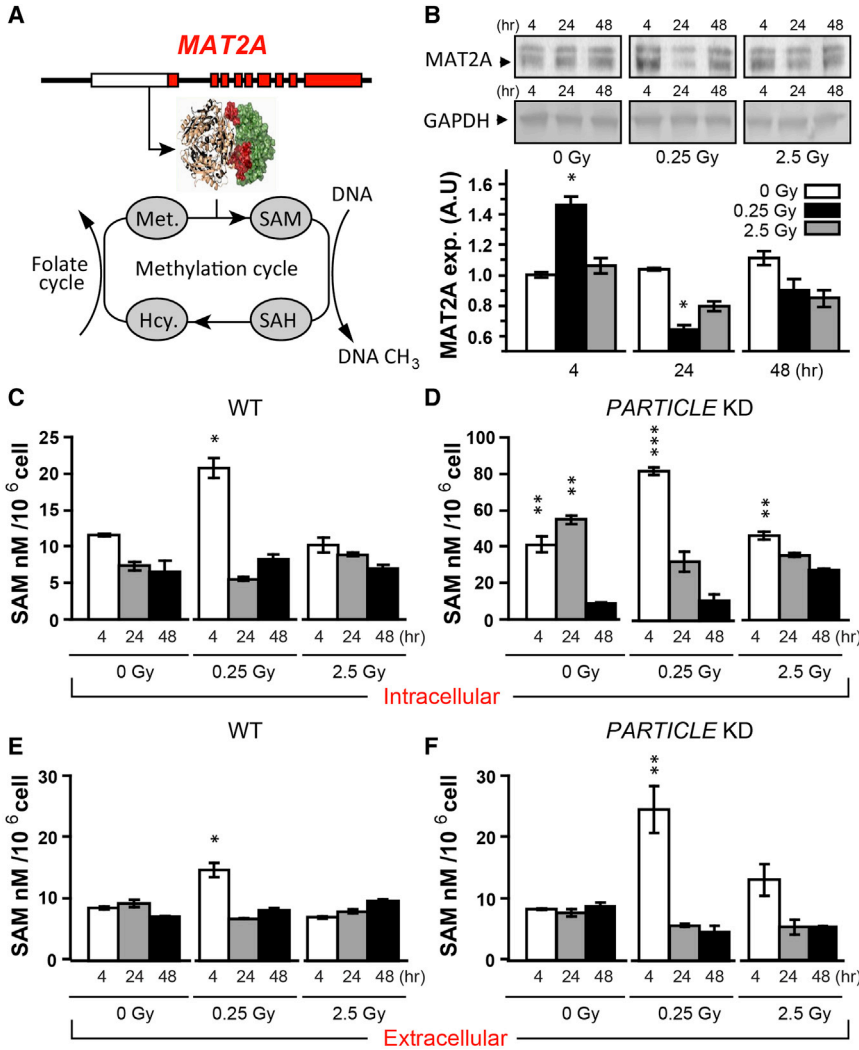

Figure 5. *PARTICLE* Knockdown Enhances Expression of the Catalytic Subunit of MAT and Increases Intracellular and Extracellular SAM Availability

(A) Diagram represents *MAT2A* (red) and its promoter (white) (top). Schematic diagram depicts an overview of the role of *MAT2A* in the methylation cycle. Structural model of MAT (González et al., 2012) indicates the catalytic region encoded by *MAT2A* (brown, middle). Overview of the cyclical methylation and folate pathways (bottom) is shown. MAT catalyzes the production of SAM from methionine (Met.) (ATP and water not shown). SAM as universal methyl donor enables protein, lipids (not shown), and DNA methyltransfereases to methylate their respective substrates.

(B) Representative western blots show MAT2A catalytic subunit expression in MDA-MB-361 at 4, 24, and 48 hr after 0.25 Gy, 2.5 Gy, or sham irradiation exposure (top) with GAPDH endogenous loading control (bottom). The samples derive from the same experiment and gels/blots were processed in parallel. Plots of MAT2A expression (AUs, n = 3) show a significant increase 4 hr following 0.25 Gy low-dose irradiation.

(C and D) Intracellular human SAM levels in MDA-MB-361 (NT controls [Wild-type, WT], C) or *PARTICLE* KD (D, per 10^6 cells) at 4, 24, and 48 hr after sham irradiation (left), 0.25 Gy (middle), or 2.5 Gy (right). Note the significant increase in intracellular SAM in *PARTICLE* KD cells and 4 hr following 0.25 Gy exposure (asterisks).

(E and F) Extracellular human SAM in tissue culture media at 4, 24, and 48 hr after sham irradiation (left), 0.25 Gy (middle), or 2.5 Gy (right) in NT controls (WT, E) or *PARTICLE* KD (F) MDA-MB-361. Data are represented as mean ± SEM. Note the increased extracellular SAM levels 4 hr following 0.25 Gy exposure (asterisks).

$p \leq 0.05$) was found only at the 4 hr time point. These findings highlight the consequences of *PARTICLE* suppression of *MAT2A* on SAM availability and the buffering of the radiation effect by control of SAM over-production.

PARTICLE Controls the Methylation Status of the *MAT2A* Promoter CpG Island

The *MAT2A* promoter contains a CpG island (annotated 108368) of 1,288 bp located on chromosome 2: 85765695–85766983 (NCBI *Homo sapiens* build number 37 version 2). The transcription initiation site for *MAT2A* resides within this region at position chromosome 2: 85766100 orientated in a forward direction (NCBI refseq NM_005911). The sequence for *PARTICLE* also overlaps this CpG island from position chromosome 2: 85765818 for 123 bp, orientated in the antisense complementary direction (Figure 6A, top).

CpG island 108368 was almost totally un-methylated (>99.7% ± 0.2%) in sham-irradiated MDA-MB-361 cells (Figure 6A, bottom left). Following exposure to 0.25 or 2.5 Gy irradiation, the CpG island 108368 became progressively methylated over the next 48 hr. Differing levels of methylation were revealed following the two irradiation doses. After low-dose exposure, CpG island 108368 remained unmethylated up to 4 hr (>99.9% ± 0.01%), but became methylated by 24 hr (62% ± 3%) increasing to 85 ± 4% by 48 hr (Figure 6A, bottom middle). Following 2.5 Gy irradiation, methylation occurred earlier (16% ± 2%), appearing by 4 hr (Figure 6A, bottom right). While methylation status increased to 49% ± 2% and 59% ± 3% for 24 and 48 hr, respectively, these levels were lower than those evoked after low-dose (0.25 Gy) irradiation exposure (Figure 6A, bottom right).

In MDA-MB-361 with *PARTICLE* knockdown (Figure 6B, top), the CpG island 108368 remained unmethylated under sham-irradiated conditions, similar to that described for cells with normal *PARTICLE* expression (Figure 6B, bottom left). However, following low-dose (0.25 Gy) irradiation, the CpG island 108368 stayed un-methylated (>99.5%) in the absence of *PARTICLE* up to 4 hr, similar to non-transduced cells, and remained un-methylated up to 24 hr (>99%); methylation began only at 48 hr, reaching 57% ± 3% (28% ± 2% lower level than in non-transduced cells; Figure 6B, bottom middle). After 2.5 Gy exposure,

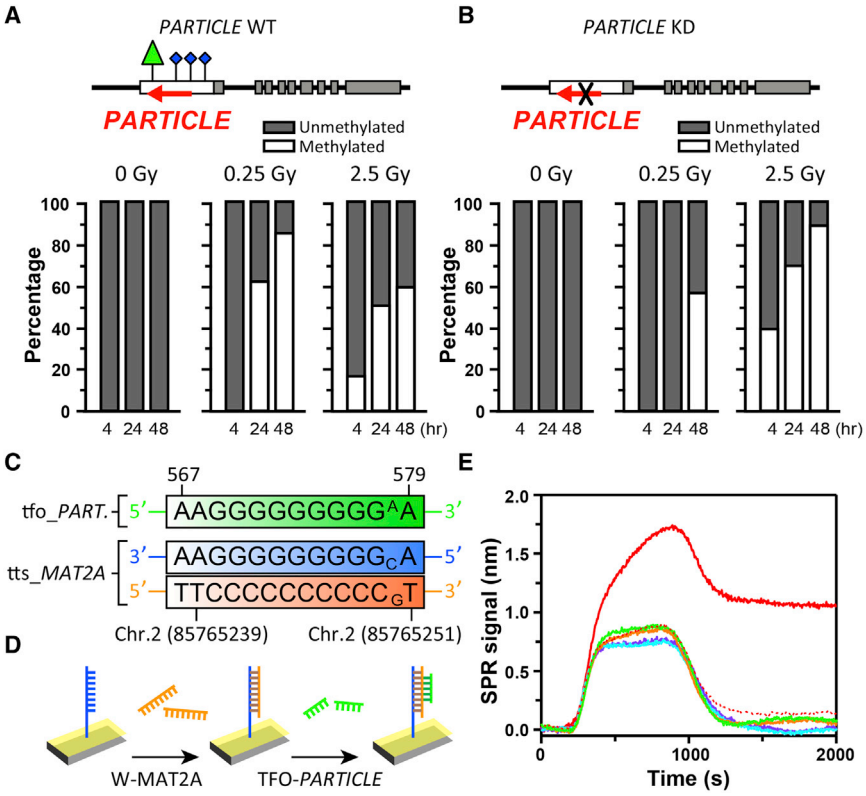

Figure 6. *PARTICLE* Influences the Methylation Status of a CpG Island and Undergoes Triplex Formation with the *MAT2A* Promoter

(A and B) (A) (Top) Schematic diagram shows position of the CpG island within the *MAT2A* promoter (blue posts). (A and B) (Top) *MAT2A* (gray) and its promoter (white) where *PARTICLE* is transcribed in an antisense direction (red arrow pointing left) are shown. Triplex formation point is upstream of the CpG island (green triangle). (A and B) (Bottom) Composite histograms show percentage unmethylation (gray) and/or methylation (white) of the CpG island within the *MAT2A* promoter after sham irradiation (left) or 4, 24, and 48 hr following exposure to 0.25 Gy (middle) or 2.5 Gy (right). Experiments (n = 3) were conducted using genomic DNA extracted from MDA-MB-361 or MDA-MB-361 with *PARTICLE* KD (B).

(C) Sequence and predicted triplex target site in the *MAT2A* locus. Triplex-forming oligonucleotide (TFO) purine-motif within *PARTICLE* (tfo_*PART.*) was identified using Triplexator software to target the unique triplex target site (TTS) in *MAT2A* (tts_MAT2A) to form a triple helix. Superscript base indicates a mismatch in the sequence.

(D) Schematic diagram depicting the in vitro demonstration of DNA:RNA triplex structure between *MAT2A* and *PARTICLE*. Various RNA oligos covering the predicted triplex-forming motif (TFO-RNA, green comb) and its context within *PARTICLE* (Table S3) were tested for triplex interaction with the *MAT2A* duplex monolayer (W-MAT2A, blue and brown combs) previously formed on the gold SPR chip.

(E) Representative sensorgram showing the specificity of triplex detection by virtue of the differential between the signal of the TFO-RNA (red line) versus the signal provided by the other RNAs tested within the context of the *PARTICLE* sequence. This TFO-RNA signal is also specific in that it requires prior formation of the duplex. Thus, only a minimal spectral shift is generated by the TFO-RNA oligonucleotide injected over the receptor without previous formation of the duplex DNA (dashed red line in sensorgram). All experiments were performed in triplicate. See also Table S3.

profiles similar to non-transduced MDA-MB-361 were revealed, although the percentage values were consistently higher (22%–30%) for all time points tested (Figure 6B, bottom right). The dose correlation between methylation and *PARTICLE* expression suggests the lncRNA may be influencing the methylation status of the *MAT2A* CpG island 24 hr after low-dose irradiation, a time when *PARTICLE* expression is elevated and *MAT2A* transcription is suppressed.

PARTICLE and *MAT2A* Form a Triplex Structure

A region (chromosome 2: 85765239–85765251) 456 bp upstream of the CpG island 108368 (described above) was identified in silico, where triplex-forming oligonucleotides within *PARTICLE* were predicted to bind upstream of a CpG island that is located in the promoter of *MAT2A* (Figures 6A [green triangle] and 6C). Computational modeling indicated that triplex formation between *PARTICLE* and this site was highly probable (score rate = 12, error rate = 0.007) (Buske et al., 2012). Surface plasmon resonance (SPR) was used to confirm that *PARTICLE* indeed interacts with *MAT2A* via a triplex mechanism. A panel of RNA oligonucleotides covering the predicted triplex-forming motif (TFO-RNA) within *PARTICLE* was tested (Table S3). A significant spectral shift occurred only with the TFO-RNA (i.e., 1.1 ± 0.05 nm, p = 0.0000377, t stat. = 115.2) (Figure 6E). Moreover, addition of the TFO-RNA to the receptor *MAT2A* without prior formation of the DNA duplex (Figure 6E) provided negligible signal (i.e., 0.09 ± 0.05 nm, p > 0.05). The resulting RNA-DNA triplex may govern the CpG island methylation to instigate transcriptional suppression of *MAT2A*.

PARTICLE Associates with Myb, G9a Lysine Methyltransferase, and the Polycomb Repressor Complex Subunit SUZ12

Chromatin immunoprecipitation (ChIP) of protein interaction partners with *PARTICLE* was performed using cross-linked chromatin isolated from irradiated MDA-MB-361 (24 hr after 0.25 Gy). Differential occupancy analysis of qPCR data revealed that the increase of *PARTICLE* at the Myb-, G9a lysine methyltransferase-, and SUZ12-binding sites was 1.3 ± 0.1, 4.1 ± 0.3, and 9.2 ± 0.7-fold, respectively (Figure 7A). Pull-down of in vitro transcribed biotinylated *PARTICLE* confirmed the association with these nuclear proteins (isolated from MDA-MB-361 24 hr after 0.25 Gy irradiation) (Figure 7B). An electrophoretic mobility shift was identified in the presence of *PARTICLE* (±biotinylation) and the polycomb repressor complex subunit SUZ12 peptide. Binding specificity was demonstrated by increasing concentrations of unlabeled *PARTICLE* (up to 1,000-fold molar excess) that significantly diminished the

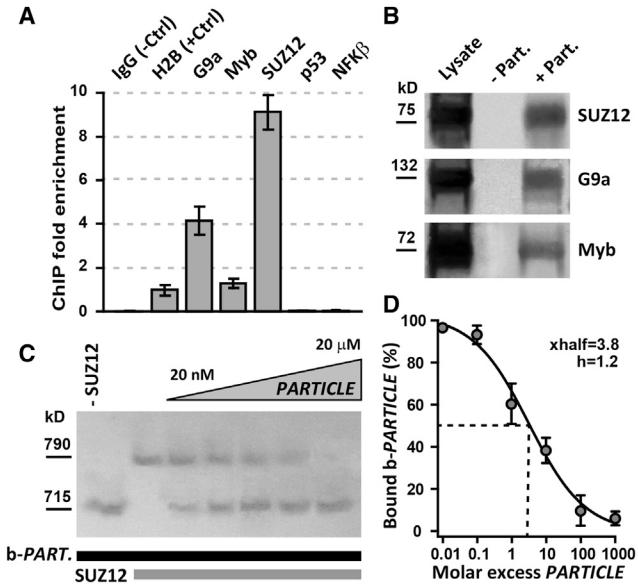

Figure 7. *PARTICLE* Associates with Myb, Lysine Methyltransferase G9a, and the Polycomb Repressor Complex Subunit SUZ12

(A) Histograms show fold increase in *PARTICLE* from qPCR expression analysis of chromatin immunoprecipitated with various antibodies, including anti-Myb, anti-G9a, and anti-SUZ12 (see Supplemental Experimental Procedures for details).

(B) Representative western blots of eluted fractions (streptavidin bead purified) probed with anti-Myb, anti-G9a, and anti-SUZ12. Biotinylated in vitro transcribed *PARTICLE* was used to pull down Myb, G9a, and SUZ12 from MDA-MB-361 (24 hr after 0.25 Gy irradiated) nuclear extracts. (Lane 1) Protein detection in nuclear lysate input; (lane 2) absence of signal in the absence of biotinylated *PARTICLE*; (lane 3) Myb, G9a, and SUZ12 detected in nuclear extracts following in vitro transcribed biotinylated *PARTICLE* pull-down and streptavidin bead elution.

(C) Representative nucleotide retardation gel (6%) of electrophoretic mobility shift assay involving binding reactions containing biotinylated *PARTICLE* (b-PART., 10 nM), ± SUZ12 peptide (2.5 μM), and increasing concentrations of unlabeled *PARTICLE* (20 nM to 20 μM) in the presence of 6.25 mM KCl is shown.

(D) Hill slope depicts the percentage of biotinylated *PARTICLE* (b-*PARTICLE*) bound to the SUZ12 peptide in the presence of molar excess of unlabeled *PARTICLE*. Data are represented as mean ± SEM.

amount of SUZ12-bound biotinylated *PARTICLE* (Figures 7C and 7D). These data show that *PARTICLE* interacts directly with PRC2 via the SUZ12 subunit. It suggests that *PARTICLE* functions, in part with epigenetic silencing complexes, to curb possible overexpression of *MAT2A* (and hence over-production of SAM and DNA methylation) following exposure to ionizing radiation.

DISCUSSION

This study introduces *PARTICLE*, an lncRNA tuner of cellular methylation following radiation exposure. An active silencing mechanism of *MAT2A* transcription by nuclear *PARTICLE* is observed, consisting of a physical crosstalk between chromosomal DNA and lncRNA leading to DNA duplex-lncRNA triplex formation, gene-silencing complex interaction, and promoter CpG island methylation. Moreover, cytosolic *PARTICLE* levels become dramatically increased following cellular irradiation amid juxtaposition with *MAT2A* transcripts, which most likely precedes their extracellular export.

MAT is a critical cellular enzyme that catalyzes the formation of SAM, the principal methyl donor, with *MAT2A* encoding the catalytic (α2) subunit of the widely distributed MAT isozyme (MATII) (Alvarez et al., 1993; Kotb et al., 1997). *PARTICLE* is transcribed in an antisense orientation to the forward plus strand from the *MAT2A* promoter. Our findings show that *MAT2A* transcription is activated much earlier than *PARTICLE,* within 4 hr following low-dose radiation exposure. This is accompanied by concomitant increases in translation and production of both intracellular and extracellular SAM. In the artificial absence of *PARTICLE,* transcriptional repression of *MAT2A* becomes diminished, resulting in elevated intracellular SAM levels, including an overshoot in irradiated *PARTICLE*-deficient cells. These results imply that *PARTICLE* directly influences the methylation cycle responsible for the conversion of methionine via SAM and s-adenosylhomocysteine (SAH) into homocysteine. As SAM is the methyl donor for multiple detoxifying methylation reactions, it is not surprising that it becomes elevated following genotoxic exposure, such as irradiation, and that it must be removed once the radiation response is completed.

Accumulating evidence suggests that long antisense ncRNAs function as epigenetic regulators of balanced transcription (Morris, 2009). This may be the principal pathway evoked by *PARTICLE* for modulating *MAT2A* expression according to selective pressures, i.e., irradiation, placed on the cell. *PARTICLE* might serve to keep in check excess availability of methyl groups required for increased DNA damage repair activity following radiation exposure. This response is most likely instigated by the upregulation of *PARTICLE* operating as a silencer through triplex (RNA:DNA:DNA) formation within the CpG island shore region (456 bp upstream of the CpG island) of the *MAT2A* promoter. While a similar triplex riboswitch has been identified upstream of *MAT2A* across a taxonomically wide range of bacteria, no mammalian evidence exists to date (Conrad, 2014). It can be inferred that human *PARTICLE* offers such a platform for controlling SAM production.

PARTICLE serves as a protein-binding platform, thereby enabling *cis* regulation of *MAT2A* transcription. *PARTICLE* interacts with the myeloblastosis (Myb) proto-oncogene transcription factor that previously has been implicated in *MAT2A* upregulation in human hepatocellular carcinomas and tumorigenesis (Yang et al., 2001). The lysine DNA methyltransferase (G9a) methylates H3K9 and H3K27 to silence transcription (Tachibana et al., 2001), and we also found G9a associating with *PARTICLE* in this study. The PRC2 complex catalyzes trimethylation of H3K27 and mediates transcriptional repression (Surface et al., 2010). A number of lncRNAs have been shown to interact with PRC2 to regulate target gene expression (Wang and Chang, 2011). Moreover, this report shows direct interaction with PRC2 and a radiation-responsive triplex-forming lncRNA, *PARTICLE*. Interestingly, a recent report demonstrated that G9a and PRC2 interact and co-localize genome-wide (Mozzetta et al., 2014). It could be proposed that *PARTICLE* binds SUZ12 and competes for PRC2 binding at target sites following

irradiation exposure. Alternatively, *PARTICLE* may aid in the recruitment of PRC2 to repress *MAT2A*, as loss of *PARTICLE* might fail to silence overactive *MAT2A* transcription in response to irradiation insult. Further studies will be necessary to fully elucidate this function, although our work suggests that *PARTICLE* mediates *MAT2A* suppression via potential epigenetic regulatory mechanisms.

It is recognized that location within the cell is an important determinant in understanding the functional roles of lncRNAs (van Heesch et al., 2014), suggesting they may play different roles depending on their sub-cellular compartment context. We have identified such a process as a possible second role for *PARTICLE* in response to low-dose irradiation. While nuclear *PARTICLE* actively represses *MAT2A*, cytosolic *PARTICLE* becomes enriched and appears to associate with cytosolic *MAT2A* transcripts, predominantly after irradiation exposure (4 hr). This could serve as an additional mechanism of *MAT2A* repression, with *PARTICLE* regulating its availability for translation.

While it is generally accepted that microRNA and mRNA can be transferred between mammalian cells by an exosome-based transport mechanism (Lässer et al., 2011), this study has identified an lncRNA in exosomes generated from in vitro, ex vivo, and in vivo irradiation. It is tempting to speculate that the detection of *PARTICLE* in plasma exosomes indicates that they serve as vectors for genetic communication between cells in distant organs. Although this suggest that *PARTICLE* may have the capacity to affect the phenotype of recipient cells, to date no mechanistic basis is known (Kadhim et al., 2013).

The roles of lncRNA in the DNA-damage/repair response are only beginning to be unraveled. Importantly, the inverse dose response exhibited by *PARTICLE* to radiation challenges the perception that all events following exposure show a linear escalation with increased doses. While their crucial existence is now un-disputed, no doubt the long non-coding genome will continue to surprise and reveal unexpected layers of cellular regulatory complexity.

EXPERIMENTAL PROCEDURES

Human lncRNA Microarray Analysis

Differentially expressed lncRNAs were identified through fold change and volcano plot filtering between samples. Genomic location was used to select for regulated intragenic lncRNAs.

Propagation and Maintenance of Cell Lines

MDA-MB-361, HEK293, U2OS, T47D, and HUVEC were propagated as described in the Supplemental Experimental Procedures. All cells were genotyped to confirm identity.

Irradiation

All irradiations were performed using a closed HWM-D 2000 unit (Siemens, 10-cm height and 33-cm circumference) delivering Cesium 137 gamma rays at a dose rate of 0.0082 Gy/s. Calibration was performed by the Research Unit of Medical Radiation Physics and Diagnostics (Helmholtz Zentrum Munich).

Ethical Approval

Samples from human subjects were obtained with informed consent. The Ethikkommission der Medizinischen Fakultat der Ludwig-Maximilian-Universität München, Germany, approved the study.

Isolation of Exosomes from Human Blood Plasma

Exosomes were isolated from human plasma of healthy donors by differential centrifugation as described in the Supplemental Experimental Procedures and as previously reported (Théry et al., 2006).

Head and Neck Squamous Cell Carcinoma Patients

The details of patient treatment and plasma isolation have been reported previously (Summerer et al., 2013).

Triplex SPR Assay

All SPR experiments were performed using a previously reported (Carrascosa et al., 2014; Sina et al., 2014) custom-made SPR platform.

ChIP

Experiments were performed using an EpiTect ChIP kit (QIAGEN, 334471) per the manufacturer's instructions. Immunoprecipitation involved the following ChIP-grade antibodies: anti-Myb, anti-KMT1C/G9a, anti-NF-κB p105/p50, anti-p53, anti-SUZ12, anti-histone H2B (positive control), and normal IgG (negative control). See the Supplemental Experimental Procedures for further details.

RNA Pull-Down

See the Supplemental Experimental Procedures for experimental details.

Electrophoretic Mobility Shift Assay

Experiments were carried out per the manufacturer's instructions (Thermo Scientific, 20158) with the inclusion of 6.25 mM KCl in the binding reactions and electrophoresis through a 6% pre-cast nucleotide retardation gel.

Statistical Analysis

Values in the text are expressed as the mean ± SEM and n refers to the number of independent data. Triplex t statistic was tested using hypothesis parameters (HA: $\mu T - \mu C > 0$) and Origin 7 software. Differences between means were tested using the Student's t test with p values < 0.05 taken to indicate statistical significance.

ACCESSION NUMBERS

The Gene Expression Omnibus (GEO) accession number for the human lncRNA microarray data reported in this paper is GSE67008.

SUPPLEMENTAL INFORMATION

Supplemental Information includes Supplemental Experimental Procedures, four figures, and three tables and can be found with this article online at http://dx.doi.org/10.1016/j.celrep.2015.03.043.

AUTHOR CONTRIBUTIONS

V.B.O. designed and performed experiments, interpreted results, and wrote the paper. S.V.O. performed microscopy, graphics, and data analysis. L.G.C. performed in vitro triplex experiments. F.A.B. designed and implemented the Triplexator software. V.R. interpreted data and corrected the manuscript. M.N. and S.M. provided valuable samples, interpreted data, and corrected the manuscript. M.T. supervised the triplex experiments. N.A. performed lentiviral preparations, interpreted results, corrected the manuscript, and supervised the project. M.J.A. designed the project, contributed to the experimental strategies, interpreted data, corrected the manuscript, coordinated the project, and directed the research.

ACKNOWLEDGMENTS

The authors thank Mr. Michael Salomon (Sirion Biotech GmbH, Germany) for helpful advice on shRNA interference and secondary structure prediction analysis. This work was supported by the EURATOM Fission, European Commission 7th Framework Programme, Dark.Risk project (contract number 323216).

L.G.C. is supported by a University of Queensland fellowship (contract number 2012001456).

Received: August 28, 2014
Revised: January 31, 2015
Accepted: March 16, 2015
Published: April 16, 2015

REFERENCES

Alvarez, L., Corrales, F., Martín-Duce, A., and Mato, J.M. (1993). Characterization of a full-length cDNA encoding human liver S-adenosylmethionine synthetase: tissue-specific gene expression and mRNA levels in hepatopathies. Biochem. J. *293*, 481–486.

Amaral, P.P., Clark, M.B., Gascoigne, D.K., Dinger, M.E., and Mattick, J.S. (2011). lncRNAdb: a reference database for long noncoding RNAs. Nucleic Acids Res. *39*, D146–D151.

Anastasov, N., Höfig, I., Vasconcellos, I.G., Rappl, K., Braselmann, H., Ludyga, N., Auer, G., Aubele, M., and Atkinson, M.J. (2012). Radiation resistance due to high expression of miR-21 and G2/M checkpoint arrest in breast cancer cells. Radiat. Oncol. *7*, 206.

Azzalin, C.M., Reichenbach, P., Khoriauli, L., Giulotto, E., and Lingner, J. (2007). Telomeric repeat containing RNA and RNA surveillance factors at mammalian chromosome ends. Science *318*, 798–801.

Bertone, P., Stolc, V., Royce, T.E., Rozowsky, J.S., Urban, A.E., Zhu, X., Rinn, J.L., Tongprasit, W., Samanta, M., Weissman, S., et al. (2004). Global identification of human transcribed sequences with genome tiling arrays. Science *306*, 2242–2246.

Buske, F.A., Bauer, D.C., Mattick, J.S., and Bailey, T.L. (2012). Triplexator: detecting nucleic acid triple helices in genomic and transcriptomic data. Genome Res. *22*, 1372–1381.

Campbell, S., Ismail, I.H., Young, L.C., Poirier, G.G., and Hendzel, M.J. (2013). Polycomb repressive complex 2 contributes to DNA double-strand break repair. Cell Cycle *12*, 2675–2683.

Carrascosa, L.G., Sina, A.A., Palanisamy, R., Sepulveda, B., Otte, M.A., Rauf, S., Shiddiky, M.J., and Trau, M. (2014). Molecular inversion probe-based SPR biosensing for specific, label-free and real-time detection of regional DNA methylation. Chem. Commun. (Camb.) *50*, 3585–3588.

Chaumeil, J., Le Baccon, P., Wutz, A., and Heard, E. (2006). A novel role for Xist RNA in the formation of a repressive nuclear compartment into which genes are recruited when silenced. Genes Dev. *20*, 2223–2237.

Conrad, N.K. (2014). The emerging role of triple helices in RNA biology. Wiley Interdiscip. Rev. RNA *5*, 15–29.

González, B., Garrido, F., Ortega, R., Martínez-Júlvez, M., Revilla-Guarinos, A., Pérez-Pertejo, Y., Velázquez-Campoy, A., Sanz-Aparicio, J., and Pajares, M.A. (2012). NADP+ binding to the regulatory subunit of methionine adenosyltransferase II increases intersubunit binding affinity in the hetero-trimer. PLoS ONE *7*, e50329.

Gupta, R.A., Shah, N., Wang, K.C., Kim, J., Horlings, H.M., Wong, D.J., Tsai, M.C., Hung, T., Argani, P., Rinn, J.L., et al. (2010). Long non-coding RNA HOTAIR reprograms chromatin state to promote cancer metastasis. Nature *464*, 1071–1076.

Huarte, M., and Rinn, J.L. (2010). Large non-coding RNAs: missing links in cancer? Hum. Mol. Genet. *19* (*R2*), R152–R161.

Hung, T., Wang, Y., Lin, M.F., Koegel, A.K., Kotake, Y., Grant, G.D., Horlings, H.M., Shah, N., Umbricht, C., Wang, P., et al. (2011). Extensive and coordinated transcription of noncoding RNAs within cell-cycle promoters. Nat. Genet. *43*, 621–629.

Kadhim, M., Salomaa, S., Wright, E., Hildebrandt, G., Belyakov, O.V., Prise, K.M., and Little, M.P. (2013). Non-targeted effects of ionising radiation-Implications for low dose risk. Mutat. Res. *752*, 84–98.

Kotb, M., Mudd, S.H., Mato, J.M., Geller, A.M., Kredich, N.M., Chou, J.Y., and Cantoni, G.L. (1997). Consensus nomenclature for the mammalian methionine adenosyltransferase genes and gene products. Trends Genet. *13*, 51–52.

Lässer, C., Alikhani, V.S., Ekström, K., Eldh, M., Paredes, P.T., Bossios, A., Sjöstrand, M., Gabrielsson, S., Lötvall, J., and Valadi, H. (2011). Human saliva, plasma and breast milk exosomes contain RNA: uptake by macrophages. J. Transl. Med. *9*, 9.

Margueron, R., and Reinberg, D. (2011). The Polycomb complex PRC2 and its mark in life. Nature *469*, 343–349.

Mato, J.M., Alvarez, L., Ortiz, P., and Pajares, M.A. (1997). S-adenosylmethionine synthesis: molecular mechanisms and clinical implications. Pharmacol. Ther. *73*, 265–280.

Morgan, W.F., and Sowa, M.B. (2015). Non-targeted effects induced by ionizing radiation: mechanisms and potential impact on radiation induced health effects. Cancer Lett. *356*, 17–21.

Morris, K.V. (2009). Long antisense non-coding RNAs function to direct epigenetic complexes that regulate transcription in human cells. Epigenetics *4*, 296–301.

Mozzetta, C., Pontis, J., Fritsch, L., Robin, P., Portoso, M., Proux, C., Margueron, R., and Ait-Si-Ali, S. (2014). The histone H3 lysine 9 methyltransferases G9a and GLP regulate polycomb repressive complex 2-mediated gene silencing. Mol. Cell *53*, 277–289.

Mullenders, L., Atkinson, M., Paretzke, H., Sabatier, L., and Bouffler, S. (2009). Assessing cancer risks of low-dose radiation. Nat. Rev. Cancer *9*, 596–604.

Özgür, E., Mert, U., Isin, M., Okutan, M., Dalay, N., and Gezer, U. (2013). Differential expression of long non-coding RNAs during genotoxic stress-induced apoptosis in HeLa and MCF-7 cells. Clin. Exp. Med. *13*, 119–126.

Pluder, F., Barjaktarovic, Z., Azimzadeh, O., Mörtl, S., Krämer, A., Steininger, S., Sarioglu, H., Leszczynski, D., Nylund, R., Hakanen, A., et al. (2011). Low-dose irradiation causes rapid alterations to the proteome of the human endothelial cell line EA.hy926. Radiat. Environ. Biophys. *50*, 155–166.

Rinn, J.L., Kertesz, M., Wang, J.K., Squazzo, S.L., Xu, X., Brugmann, S.A., Goodnough, L.H., Helms, J.A., Farnham, P.J., Segal, E., and Chang, H.Y. (2007). Functional demarcation of active and silent chromatin domains in human HOX loci by noncoding RNAs. Cell *129*, 1311–1323.

Schoeftner, S., and Blasco, M.A. (2008). Developmentally regulated transcription of mammalian telomeres by DNA-dependent RNA polymerase II. Nat. Cell Biol. *10*, 228–236.

Sina, A.A., Carrascosa, L.G., Palanisamy, R., Rauf, S., Shiddiky, M.J., and Trau, M. (2014). Methylsorb: a simple method for quantifying DNA methylation using DNA-gold affinity interactions. Anal. Chem. *86*, 10179–10185.

Struhl, K. (2007). Transcriptional noise and the fidelity of initiation by RNA polymerase II. Nat. Struct. Mol. Biol. *14*, 103–105.

Summerer, I., Niyazi, M., Unger, K., Pitea, A., Zangen, V., Hess, J., Atkinson, M.J., Belka, C., Moertl, S., and Zitzelsberger, H. (2013). Changes in circulating microRNAs after radiochemotherapy in head and neck cancer patients. Radiat. Oncol. *8*, 296.

Surface, L.E., Thornton, S.R., and Boyer, L.A. (2010). Polycomb group proteins set the stage for early lineage commitment. Cell Stem Cell *7*, 288–298.

Tachibana, M., Sugimoto, K., Fukushima, T., and Shinkai, Y. (2001). Set domain-containing protein, G9a, is a novel lysine-preferring mammalian histone methyltransferase with hyperactivity and specific selectivity to lysines 9 and 27 of histone H3. J. Biol. Chem. *276*, 25309–25317.

Théry, C., Amigorena, S., Raposo, G., and Clayton, A. (2006). Isolation and characterization of exosomes from cell culture supernatants and biological fluids. Curr. Protoc. Cell Biol. *Chapter 3*, Unit 3.22.

Tsai, M.C., Manor, O., Wan, Y., Mosammaparast, N., Wang, J.K., Lan, F., Shi, Y., Segal, E., and Chang, H.Y. (2010). Long noncoding RNA as modular scaffold of histone modification complexes. Science *329*, 689–693.

van Heesch, S., van Iterson, M., Jacobi, J., Boymans, S., Essers, P.B., de Bruijn, E., Hao, W., MacInnes, A.W., Cuppen, E., and Simonis, M. (2014). Extensive localization of long noncoding RNAs to the cytosol and mono- and polyribosomal complexes. Genome Biol. *15*, R6.

Waldren, C.A., Vannais, D.B., and Ueno, A.M. (2004). A role for long-lived radicals (LLR) in radiation-induced mutation and persistent chromosomal

instability: counteraction by ascorbate and RibCys but not DMSO. Mutat. Res. *551*, 255–265.

Wan, G., Mathur, R., Hu, X., Liu, Y., Zhang, X., Peng, G., and Lu, X. (2013). Long non-coding RNA ANRIL (CDKN2B-AS) is induced by the ATM-E2F1 signaling pathway. Cell. Signal. *25*, 1086–1095.

Wang, K.C., and Chang, H.Y. (2011). Molecular mechanisms of long noncoding RNAs. Mol. Cel1 *43*, 904–914.

Wang, X., Arai, S., Song, X., Reichart, D., Du, K., Pascual, G., Tempst, P., Rosenfeld, M.G., Glass, C.K., and Kurokawa, R. (2008). Induced ncRNAs allosterically modify RNA-binding proteins in cis to inhibit transcription. Nature *454*, 126–130.

Yang, H., Huang, Z.Z., Wang, J., and Lu, S.C. (2001). The role of c-Myb and Sp1 in the up-regulation of methionine adenosyltransferase 2A gene expression in human hepatocellular carcinoma. FASEB J. *15*, 1507–1516.

Zhang, L.F., Huynh, K.D., and Lee, J.T. (2007). Perinucleolar targeting of the inactive X during S phase: evidence for a role in the maintenance of silencing. Cell *129*, 693–706.